11226 *Inorg. Chem.* **2009**, *48*, 11226–11235
DOI: 10.1021/ic901710x

Inorganic Chemistry
Article

From Monomers to Geometry-Constrained Molecules: One Step Further Toward Cyanide Bridged Wires

Pablo Albores,[†] Leonardo D. Slep,[†] Livia S. Eberlin,[§] Yuri E. Corilo,[§] Marcos N. Eberlin,[§] Guillermo Benítez,[‡] Maria E. Vela,[‡] Roberto C. Salvarezza,[‡] and Luis M. Baraldo*[,†]

[†]*Departamento de Química Inorgánica, Analítica y Química Física, INQUIMAE-CONICET, Facultad de Ciencias Exactas y Naturales, Universidad de Buenos Aires, Pabellón 2, 3er piso, Ciudad Universitaria, C1428EHA Buenos Aires, Argentina,* [‡]*Instituto de Investigaciones Fisicoquímicas Teóricas y Aplicadas, INIFTA-CONICET-UNLP, Casilla de Correo 16, Sucursal 4, 1900 La Plata, Argentina, and* [§]*ThoMSon Mass Spectrometry Laboratory, Institute of Chemistry, University of Campinas − UNICAMP Campinas, São Paulo 13083-970, Brazil*

Received August 28, 2009

We report on the synthesis and properties of a family of linear cyanide bridged mixed-valence heptanuclear complexes with the formula: *trans*-$[L_4Ru^{II}\{(\mu\text{-NC})Fe^{III}(NC)_4(\mu\text{-CN})Ru^{II}L'_4(\mu\text{-NC})Fe^{III}(CN)_5\}_2]^{6-}$ (with L and L′ a *para* substituted pyridine). We also report on the properties of a related pentanuclear complex. These oligomers were purified by size exclusion chromatography, characterized by electrospray ionization (ESI) mass spectrometry and elemental analysis, and their linear shape was confirmed by scanning tunneling microscopy (STM). These complexes present a rich electrochemistry associated with the seven redox active centers. The redox potential split of identical fragments indicates that there is considerable communication along the cyanide bridged backbone of the compounds, even for centers more than 3 nm apart. This small attenuation of the interaction at long distances make these cyanide bridged compounds good candidates for molecular wires. Interestingly, the extent of the communication depends on the relative energy of the fragments, as evaluated by their redox potentials, providing a guide for improvement of this interesting property.

Introduction

In the past decades, a few dozen of mixed valence dinuclear[1−6] and trinuclear[2−5,7,8] cyanide bridged transition metal complexes have been prepared. In spite of the number of important advances in this field, the amount of well characterized mixed valence clusters with high nuclearity is still very limited, comprising a few square,[9] cubic[10] and globular clusters.[11] Linear polymetallic cyanide bridged complexes are even less common.[3,12] The interest in the linear geometry has increased in the context of molecular electronics owing to their potential application as "molecular wires", consequently the synthesis and characterization of

*To whom correspondence should be addressed. E-mail: baraldo@qi.fcen.uba.ar.

(1) (a) Vogler, A.; Kisslinger, J. *J. Am. Chem. Soc.* **1982**, *104*, 2311–2312. (b) Siddiqui, S.; Henderson, W. W.; Shepherd, R. E. *Inorg. Chem.* **1987**, *26*, 3101–3107. (c) Vogler, A.; Osman, A. H.; Kunkely, H. *Inorg. Chem.* **1987**, *26*, 2337–2340. (d) Burewicz, A.; Haim, A. *Inorg. Chem.* **1988**, *27*, 1611–1614. (e) Cutin, E. H.; Katz, N. E. *Polyhedron* **1993**, *12*, 955–960. (f) Laidlaw, W. M.; Denning, R. G.; Verbiest, T.; Chauchard, E.; Persoons, A. *Nature* **1993**, *363*, 58–60. (g) Forlano, P.; Baraldo, L. M.; Olabe, J. A.; Della Védova, C. O. *Inorg. Chim. Acta* **1994**, *223*, 37–42. (h) Laidlaw, W. M.; Denning, R. G. *J. Chem. Soc., Dalton Trans.* **1994**, 1987–1994. (i) Laidlaw, W. M.; Denning, R. G. *Polyhedron* **1994**, *13*, 1875–1880. (j) Fagalde, F.; Katz, N. E. *Polyhedron* **1995**, *14*, 1213–1220. (k) Kunkely, H.; Pawlowski, V.; Vogler, A. *Inorg. Chim. Acta* **1994**, *225*, 327–330. (l) Forlano, P.; Cukiernik, F. D.; Poizat, O.; Olabe, J. A. *J. Chem. Soc.-Dalton Trans.* **1997**, 1595–1599. (m) Díaz, C.; Arancibia, A. *Inorg. Chim. Acta* **1998**, *269*, 246–252. (n) Geiss, A.; Vahrenkamp, H. *Inorg. Chem.* **2000**, *39*, 4029–4036. (o) Vance, F. W.; Slone, R. V.; Stern, C. L.; Hupp, J. T. *Chem. Phys.* **2000**, *253*, 313–322. (u) Baraldo, L. M.; Forlano, P.; Parise, A. R.; Slep, L. D.; Olabe, J. A. *Coord. Chem. Rev.* **2001**, *219*, 881–921. (v) Adams, C. J.; Connelly, N. G.; Goodwin, N. J.; Hayward, O. D.; Orpen, A. G.; Wood, A. J. *Dalton Trans.* **2006**, 3584–3596.

(2) (a) Bignozzi, C. A.; Roffia, S.; Scandola, F. *J. Am. Chem. Soc.* **1985**, *107*, 1644–1651. (b) Bignozzi, C. A.; Paradisi, C.; Roffia, S.; Scandola, F. *Inorg. Chem.* **1988**, *27*, 408–414.

(3) Geiss, A.; Vahrenkamp, H. *Eur. J. Inorg. Chem.* **1999**, 1793–1803.

(4) (a) Macatangay, A. V.; Endicott, J. F. *Inorg. Chem.* **2000**, *39*, 437–446. (b) Pfennig, B. W.; Fritchman, V. A.; Hayman, K. A. *Inorg. Chem.* **2001**, *40*, 255–263.

(5) Albores, P.; Slep, L. D.; Weyhermuller, T.; Baraldo, L. M. *Inorg. Chem.* **2004**, *43*, 6762–6773.

(6) Albores, P.; Rossi, M. B.; Baraldo, L. M.; Slep, L. D. *Inorg. Chem.* **2006**, *45*, 10595–10604.

(7) (a) Bignozzi, C. A.; Roffia, S.; Chiorboli, C.; Davila, J.; Indelli, M. T.; Scandola, F. *Inorg. Chem.* **1989**, *28*, 4350–4358. (b) Geiss, A.; Kolm, M. J.; Janiak, C.; Vahrenkamp, H. *Inorg. Chem.* **2000**, *39*, 4037–4043. (c) Sheng, T. L.; Appelt, R.; Comte, V.; Vahrenkamp, H. *Eur. J. Inorg. Chem.* **2003**, 3731–3737.

(8) (a) Roffia, S.; Casadei, R.; Paolucci, F.; Paradisi, C.; Bignozzi, C. A.; Scandola, F. *J. Electroanal. Chem.* **1991**, *302*, 157–171. (b) Richardson, G. N.; Brand, U.; Vahrenkamp, H. *Inorg. Chem.* **1999**, *38*, 3070–3079. (c) Appelt, R.; Vahrenkamp, H. *Inorg. Chim. Acta* **2003**, *350*, 387–398.

Published on Web 11/06/2009

Scheme 1. Sketches of the Anionic Complexes Reported in This Work

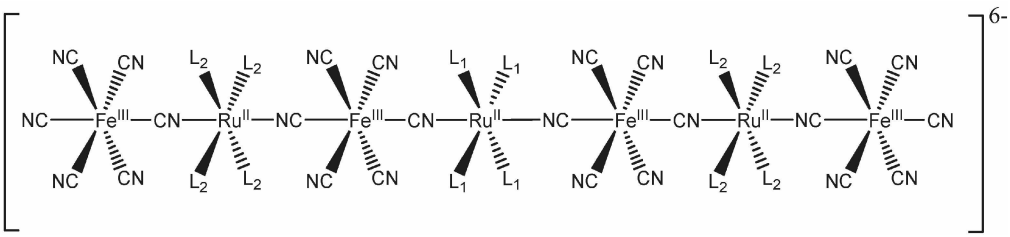

Anionic Complexes	L_1	L_2
$\mathbf{1}^{6-}$	4-methoxypyridine	pyridine
$\mathbf{2}^{6-}$		4-*tert*-butylpyridine
$\mathbf{3}^{6-}$		4-methoxypyridine
$\mathbf{4}^{6-}$	4-dimethylaminopyridine	pyridine
$\mathbf{5}^{6-}$		4-*tert*-butylpyridine
$\mathbf{6}^{6-}$		4-methoxypyridine

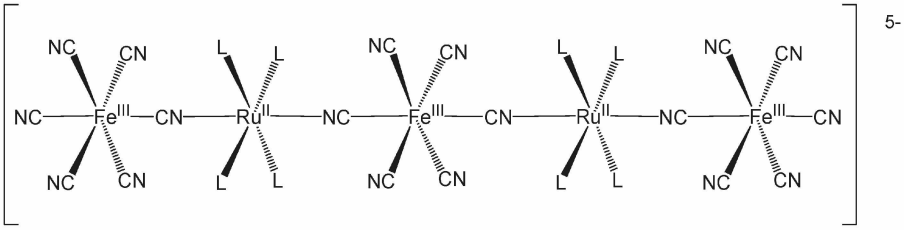

L = 4-*tert*-butylpyridine

$\mathbf{7}^{5-}$

several linear systems based on coordination complexes have been reported lately.[13,14] Focusing on the use as molecular wires, many synthetic approaches have tried to prepare oligonuclear transition metal complexes with different degrees of electronic coupling between their constituents; hence, their design relies on the known properties of dinuclear systems. Given the extensive exploration of cyanide bridged compounds, they represent an attractive starting point for the rational design of molecular wires.

But preparing such complexes is a true synthetic challenge mainly because of difficulties in controlling the length of the oligonuclear chain. The use of end-capped fragments prevents uncontrolled growth of the chain compounds, but this strategy leads to a dead end because these molecules are not suitable to be incorporated in larger units. A promising alternative is the use of geometry constrained precursors bearing open coordination sites with moderate lability. Second row transition metal complexes with *trans* configuration are well suited for these synthetic requirements.

In this work we report the synthesis and characterization of a linear oligomer family, with cyanide bridges between the metal centers, prepared by controlled reaction between the trinuclear building blocks *trans*-$[L_4Ru^{II}\{\mu\text{-}NCFe^{III}(CN)_5\}_2]^{4-}$ (L = *para* substituted pyridine) with suitable ruthenium monomeric precursors. Careful selection of the reaction conditions prevented the unwanted polymerization, yielding multiply charged (6−) anionic complexes $(\mathbf{1-6})^{6-}$ of general formula: *trans*-$[L_4Ru^{II}\{(\mu\text{-}NC)Fe^{III}(NC)_4(\mu\text{-}CN)Ru^{II}L'_4(\mu\text{-}NC)Fe^{III}(CN)_5\}_2]^{6-}$ (Scheme 1) that

(9) (b) Oshio, H.; Onodera, H.; Ito, T. *Chem.—Eur. J.* **2003**, *9*, 3946–3950. (b) Oshio, H.; Onodera, H.; Tamada, O.; Mizutani, H.; Hikichi, T.; Ito, T. *Chem.—Eur. J.* **2000**, *6*, 2523–2530.

(10) Nihei, M.; Ui, M.; Hoshino, N.; Oshio, H. *Inorg. Chem.* **2008**, *47*, 6106–6108.

(11) (a) Poulopoulou, V. G.; Taube, H.; Nunes, F. S. *Inorg. Chem.* **1999**, *38*, 2844–2850. (b) Rogez, G.; Marvilliers, A.; Rivière, E.; Audière, J.-P.; Lloret, F.; Varret, F.; Goujon, A.; Mendenez, N.; Girerd, J.-J.; Mallah, T. *Angew. Chem., Int. Ed.* **2000**, *39*, 2885–2887. (c) Rogez, G.; Marvilliers, A.; Sarr, P.; Parsons, S.; Teat, S. J.; Ricard, L.; Mallah, T. *Chem. Commun.* **2002**, 1460–1461. (d) Rogez, G.; Parsons, S.; Paulsen, C.; Villar, V.; Mallah, T. *Inorg. Chem.* **2001**, *40*, 3836–3837. (e) Rogez, G.; Riviere, E.; Mallah, T. *C. R. Chim.* **2003**, *6*, 283–290.

(12) Geiss, A.; Keller, M.; Vahrenkamp, H. *J. Organomet. Chem.* **1997**, *541*, 441–443.

(13) (a) Von Kameke, A.; Tom, G. M.; Taube, H. *Inorg. Chem.* **1978**, *17*, 1790–1796. (b) Berry, J. F.; Cotton, F. A.; Lei, P.; Lu, T. B.; Murillo, C. A. *Inorg. Chem.* **2003**, *42*, 3534–3539. (c) Robertson, N.; McGowan, C. A. *Chem. Soc. Rev.* **2003**, *32*, 96–103. (d) Cho, T. J.; Moorefield, C. N.; Hwang, S. H.; Wang, P. S.; Godinez, L. A.; Bustos, E.; Newkome, G. R. *Eur. J. Org. Chem.* **2006**, 4193–4200. (e) Flores-Torres, S.; Hutchison, G. R.; Soltzberg, L. J.; Abruna, H. D. *J. Am. Chem. Soc.* **2006**, *128*, 1513–1522. (f) Khanra, S.; Weyhermüller, T.; Bill, E.; Chaudhuri, P. *Inorg. Chem.* **2006**, *45*, 5911–5923. (g) Liu, I. P. C.; Benard, M.; Hasanov, H.; Chen, I. W. P.; Tseng, W. H.; Fu, M. D.; Rohmer, M. M.; Chen, C. H.; Lee, G. H.; Peng, S. M. *Chem.—Eur. J.* **2007**, *13*, 8667–8677. (h) Maurer, J.; Sarkar, B.; Kaim, W.; Winter, R. F.; Zalis, S. *Chem.—Eur. J.* **2007**, *13*, 10257–10272. (i) Yamamoto, Y.; Sawa, S.; Funada, Y.; Morimoto, T.; Falkenstrom, M.; Miyasaka, H.; Shishido, S.; Ozeki, T.; Koike, K.; Ishitani, O. *J. Am. Chem. Soc.* **2008**, *130*, 14659–14674.

(14) Loiseau, F.; Nastasi, F.; Stadler, A. M.; Campagna, S.; Lehn, J. M. *Angew. Chem., Int. Ed.* **2007**, *46*, 6144–6147.

were isolated as tetraphenylphosphonium (Ph_4P^+) salts. The isolation of these high nuclearity species lead us to re-examine the main byproduct in the synthesis of the trinuclear building blocks,[5] which turned out to be the pentanuclear *trans*-$[(NC)_4Fe^{III}\{(\mu\text{-}CN)Ru^{II}L_4(\mu\text{-}NC)Fe^{III}(CN)_5\}_2]^{5-}$, $\mathbf{7}^{5-}$. These oligonuclear systems are soluble in polar solvents such as methanol, opening the possibility of their complete electrochemical, spectroscopic, and mass spectrometric characterization.

Experimental Section

Materials. The complexes *trans*-$[Ru^{II}Cl_2(MeOpy)_4]$ (MeOpy = 4-methoxypyridine),[5] $[Ru^{II}(DMAP)_6]\cdot 9H_2O$ (DMAP = 4-dimethylaminopyridine),[15] $[Ph_4P]_4$*trans*-$[L_4Ru^{II}\{(\mu\text{-}NC)Fe^{III}(CN)_5\}_2]\cdot xH_2O$ (L = pyridine (py), 4-*tert*-butylpyridine (*t*Bupy), and MeOpy)[5] were prepared as previously described. Solvents for UV−visible and electrochemistry measurements were dried according to literature procedures.[16] All other reagents were obtained commercially and used as supplied. All the compounds synthesized in this work were dried in a vacuum desiccator for at least 12 h prior to characterization.

Synthesis of the Complexes. $[Ph_4P]_6$*trans*-$[(MeOpy)_4Ru^{II}\{(\mu\text{-}NC)Fe^{III}(CN)_4(\mu\text{-}CN)Ru^{II}L_4(\mu\text{-}NC)Fe^{III}(CN)_5\}_2]\cdot xH_2O$, (**1**) L = py, $x = 20$ (**2**) L = 4-*t*Bupy, $x = 18$ (**3**) L = 4-MeOpy, $x = 20$. In a typical preparation, 10 mg (0.016 mmol) of solid *trans*-$Ru^{II}(MeOpy)_4Cl_2$ were added to a solution of 0.6 g (0.25 mmol) of $[Ph_4P]_4$*trans*-$[L_4Ru^{II}\{(\mu\text{-}NC)Fe^{III}(CN)_5\}_2]\cdot xH_2O$ (L = pyridine, $x = 9$; L = 4-*t*Bupy, $x = 7$ and L = MeOpy, $x = 10$) dissolved in about 15 mL of methanol. The suspension was refluxed in the dark with vigorous stirring for about 1 h. At this point all the initial solid dissolved completely. Another 10 mg (0.016 mmol) of the solid ruthenium monomer were added, and the suspension was refluxed for an extra hour. The resulting green solution was cooled down to room temperature (RT), and the solvent was removed under reduced pressure. This solid residue was dissolved in a minimum amount of methanol, filtered, and loaded in a methanolic LH-20 Sephadex column ($l = 60$ cm, $\phi = 4$ cm). Elution with methanol afforded three main green fractions. The first one was discarded. The last fraction contained the unreacted trinuclear compound. The second fraction was collected and purified again by exclusion chromatography affording the desired product. Typical yields range between 20 and 25%. Anal. Calcd for **1** $C_{232}H_{188}N_{36}O_4P_6Fe_4Ru_3\cdot 20H_2O$: C, 60.4; H, 4.9; N, 10.9; Found: C, 60.1; H, 4.9; N, 10.5. ν (CN): 2108 (s) cm^{-1}. Anal. Calcd for **2** $C_{264}H_{252}N_{36}O_4P_6Fe_4Ru_3\cdot 18H_2O$: C, 63.0; H, 5.7; N, 10.0; Found: C, 63.1; H, 5.5; N, 9.9. ν (CN): 2106 (s) cm^{-1}. Anal. Calcd for **3** $C_{240}H_{204}N_{36}O_{12}P_6Fe_4Ru_3\cdot 20H_2O$: C, 59.3; H, 5.1; N, 10.4; Found: C, 58.8; H, 4.9; N, 11.0. ν (CN): 2107 (s) cm^{-1}.

$[Ph_4P]_6$*trans*-$[(DMAP)_4Ru^{II}\{(\mu\text{-}NC)Fe^{III}(NC)_4(\mu\text{-}CN)Ru^{II}L_4(\mu\text{-}NC)Fe^{III}(CN)_5\}_2]\cdot xH_2O$, (**4**) L = py, $x = 0$ (**5**) L = 4-*t*-Bupy, $x = 4$ (**6**) L = 4-MeOpy, $x = 4$. Typically, 26 mg (0.025 mmol) of $[Ru^{II}(DMAP)_6]Cl_2\cdot 9H_2O$ dissolved in 7 mL of methanol were mixed with a solution of 0.36 g (0.15 mmol) of $[Ph_4P]_4$*trans*-$[L_4Ru^{II}\{(\mu\text{-}CN)Fe^{III}(CN)_5\}_2]\cdot xH_2O$ (L = py, $x = 9$; L = *t*Bupy, $x = 7$ and L = 4-MeOpy, $x = 10$) in 12 mL of methanol. This solution was refluxed in the dark for 30 min. After cooling down to RT, the solvent was removed under reduced pressure, and the solid residue was loaded in a methanolic LH-20 Sephadex column ($l = 60$ cm, $\phi = 4$ cm). Elution with methanol afforded four main fractions. The first two fractions were discarded. The third green fraction was collected and repurified by the same procedure affording the desired product. The fourth fraction was also collected recovering the excess unreacted trinuclear compound. Typical yields range between 20 and 25%. Anal. Calcd for **4** $C_{236}H_{200}N_{40}P_6Fe_4Ru_3$: C, 65.8; H, 4.6; N, 13.0; Found: C, 66.6; H, 4.5; N, 13.0. ν (CN): 2037 (w) cm^{-1}, 2107 (s) cm^{-1}. Anal. Calcd for **5** $C_{268}H_{264}N_{40}P_6Fe_4Ru_3\cdot 4H_2O$: C, 66.6; H, 5.7; N, 11.6; Found: C, 66.5; H, 6.4; N, 11.6. ν (CN): 2068 (w) cm^{-1}, 2106 (s) cm^{-1}. Anal. Calcd for **6** $C_{246}H_{220}N_{40}O_8P_6Fe_4Ru_3\cdot 4H_2O$: C, 63.5; H, 4.9; N, 12.0; Found: C, 63.9; H, 5.3; N, 11.5. ν (CN): 2044 (w) cm^{-1}, 2106 (s) cm^{-1}.

$[Ph_4P]_5$*trans*-$[(NC)_4Fe^{III}\{(\mu\text{-}CN)Ru^{II}L_4(\mu\text{-}NC)Fe^{III}(CN)_5\}_2]\cdot 2H_2O$ (**7**). This compound is obtained as the main side-product of the synthesis of $[Ph_4P]_4$*trans*-$[(t\text{Bupy})_4Ru^{II}\{(\mu\text{-}CN)Fe^{III}(CN)_5\}_2]\cdot 7H_2O$ which has already been described in a previous publication.[5] It is isolated as the first major fraction eluting from the methanolic Sephadex LH-20 chromatography procedure used in the purification of the trinuclear compound. This fraction was repurified by the same technique. The Ru based yield is 10%. Anal. Calcd for **7** $C_{210}H_{204}N_{26}P_5Fe_3Ru_2\cdot 2H_2O$: C, 69.1; H, 5.7; N, 9.9; Found: C, 69.1; H, 6.3; N, 9.2. ν (CN): 2107 (s) cm^{-1}.

Aqueous solutions of the sodium salts of the reported new complexes were prepared as follows: the Ph_4P^+ salt of any of the species was dissolved in a minimum amount of acetonitrile, and solid $NaClO_4$ was added. The precipitated sodium salt was filtered off, washed with acetonitrile, and vacuum-dried. It was then redissolved in water and filtered again, quantitatively yielding the aqueous solutions for spectroscopic measurements. One-electron oxidation of **4**−**6** in methanol was performed by addition of 1 equiv of $(NH_4)_2[Ce^{IV}(NO_3)_6]$.

Physical Measurements. IR spectra were collected with a Nicolet FTIR 510P instrument, as KBr pellets. UV−visible spectra were recorded with a Hewlett-Packard 8453 diode array spectrometer in the range between 190 and 1100 nm or with a Shimadzu 3100 UV−vis/NIR for the NIR (up to 2500 nm) region. Elemental analyses were performed with a Carlo Erba 1108 analyzer. Hydration water molecules in the reported complexes were determined by thermo-gravimetric measurements with a TGA-51 Shimadzu thermo-gravimetric analyzer. The mass spectrometric measurements were performed using a high-resolution and high accuracy hybrid quadrupole (Q) and orthogonal time-of-flight (Tof) mass spectrometer (QTof from Micromass, U.K.) operating in the negative ion mode. Complexes were dissolved (1 mg/mL) in a 1:1 volume ratio methanol/acetonitrile mixture. The temperature of the nebulizer was 100 °C, and the cone voltage was 30 V. Cyclic voltammetry measurements were performed under argon with millimolar solutions of the compounds, using a PAR 273A potentiostat and a standard three electrode arrangement consisting of a glassy carbon disk (area = 9.4 mm^2) as the working electrode, a platinum wire as the counter electrode, and a reference electrode. Depending on the situation the reference electrode was a Ag/AgCl 3 M KCl standard electrode (for aqueous solutions) or a silver wire plus an internal ferrocene (Fc) standard for organic solvents. KNO_3 1 M and tetra-*N*-butylammoniumhexafluorophosphate ($TBAPF_6$) 0.1 M were used as supporting electrolytes in water and non-aqueous media respectively. All the potentials reported in this work are referenced to the standard Ag/AgCl saturated KCl electrode (0.197 V vs. NHE), the conversions being performed by using the accepted values for the Fc^+/Fc couple in different media.[17] Scanning Tunneling Microscopy (STM) imaging was performed in air in the constant current mode with a Nanoscope III microscope from Digital Instruments (Santa Barbara, CA), and by using commercial Pt−Ir tips. Typical tunneling current and bias voltage for molecular resolution were 0.1−0.2 nA and 1 V.

(15) Rossi, M. B.; Piro, O. E.; Castellano, E. E.; Alborés, P.; Baraldo, L. M. *Inorg. Chem.* **2008**, *47*, 2416–2427.

(16) Armarego, W. L. F.; Perrin, D. D., *Purification of laboratory chemicals*; 4th ed.; Butterworth-Heinemann: Woburn, MA, 1996.

(17) Noviandri, I.; Brown, K. N.; Fleming, D. S.; Gulyas, P. T.; Lay, P. A.; Masters, A. F.; Phillips, L. *J. Phys. Chem. B* **1999**, *103*, 6713–6722.

Smooth Au substrates with (111) preferential orientation (from Arrandee's) were annealed for 5 min in a butane-propane flame until the film color turned to a dark red. The Au substrates were immersed in 0.05 mM cysteamine-containing ethanolic solution for 24 h to form the SAMs (Self Assembly Monolayers). The cysteamine-covered substrates were removed from the solution, carefully rinsed with ethanol to eliminate cysteamine multilayer, rinsed with water, and finally dried under nitrogen stream. Complexes were immobilized by immersion of the cysteamine-covered Au substrates in 0.1 mM methanolic solution of the complex in the presence of a few drops of HCl for 30 min. After this procedure the Au(111) substrate was removed from the solution and carefully rinsed with Milli-Q-water and dried under nitrogen stream. AES (Auger Electron Spectroscopy) measurements were performed by using a single pass cylindrical mirror analyzer (CMA) from Physical Electronics. Cyclic voltammetry measurements of the gold surfaces containing the immobilized complexes were performed under nitrogen purged phosphate aqueous solution (pH = 3), with a three electrode arrangement consisting of the gold surface itself as the working electrode, a platinum grid as the counter electrode, and a SCE (Saturated Calomel Electrode) reference electrode.

Results

Synthesis. A family of anionic heptanuclear complexes of formula *trans*-$[L_4Ru^{II}\{(\mu\text{-NC})Fe^{III}(NC)_4(\mu\text{-CN})Ru^{II}L'_4(\mu\text{-NC})Fe^{III}(CN)_5\}_2]^{6-}$ (Scheme 1) were isolated as Ph_4P^+ salts after reaction between the mononuclear *trans*-$Ru^{II}L_4Cl_2$ or $[Ru^{II}(DMAP)_6]^{2+}$ precursors with an excess of linear trinuclear compounds *trans*-$[L_4Ru^{II}\{(\mu\text{-CN})Fe^{III}(CN)_5\}_2]^{4-}$ in refluxing methanol, followed by purification by size exclusion chromatography. In the synthesis of the respective trinuclear complex, the linear pentanuclear compound *trans*-$[(NC)_4Fe^{III}\{(\mu\text{-NC})Ru^{II}(t\text{Bupy})_4(\mu\text{-NC})Fe^{III}(CN)_5\}_2]^{5-}$ was isolated from the chromatographic purification as the main side-product, also as its Ph_4P^+ salt.[5]

Mass Spectrometric Measurements. To conclusively confirm the molecular weight, composition, connectivity, and nuclearity of the reported complexes, electrospray ionization mass spectrometry (ESI-MS) and tandem mass spectrometry (ESI-MS/MS) in the negative mode were employed (for examples of the use of ESI-MS and ESI-MS for the characterization of organometallic species see ref 18). Typically, the solvated anions $(\mathbf{1}-\mathbf{6})^{6-}$ were not detected as the naked sextuply charged gaseous species (probably because of inherent gas phase instability owing to too high charge density) but via a series of anions with reduced charge states achieved via partial protonation or ion pairing. For instance, $\mathbf{2}^{6-}$ (Figure 1a) was detected via a series of quadruply charged species: $[\mathbf{2} + 2H]^{4-}$ of m/z 668.1336, $[\mathbf{2} + H + PPh_4]^{4-}$ of m/z 752.6852, $[\mathbf{2} + 2PPh_4]^{4-}$ of m/z 837.2248, $[\mathbf{2} + 2H + PPh_4]^{4-}$ of m/z 1003.3270, and $[\mathbf{2} + H + PPh_4]^{4-}$ of m/z 1116.8060 (Figure 1a). It should be noticed that only the observed m/z value of the most abundant isotopologue ion for such multi-isotopic species forming multifaceted isotope clusters are mentioned. Other analogous gaseous species with higher degree of protonation or cationization such as, for instance, $[\mathbf{2} + 3H]^{3-}$ and Na^+ and K^+ adducts such as $[\mathbf{2} + 2Na + H]^{3-}$ or $[\mathbf{2} + K + PPh_4 + H]^{3-}$ were also detected as a function of pH and salt content. Each of such gaseous ions displays also very typical multifaceted isotope clusters with a diversity of isotopologue ions owing mainly to the multiple combinations of Ru and Fe isotopes (Figure 1b). The observed isotope cluster matches the calculated ones, and Table 1 shows, for a typical isotope cluster detected for each salt solution, the observed and calculated m/z values for their most abundant isotopologue ion. The tandem mass spectra (ESI-MS/MS) of these stable and unique gaseous ions also reveal characteristic and structurally diagnostic dissociation chemistry as Scheme 2 summarizes. For instance, one of the isotopologue ions of the major species detected for $\mathbf{2}^{6-}$, that is, $[\mathbf{2} + 2H]^{4-}$, of ca. m/z 667.1578 (the m/z value

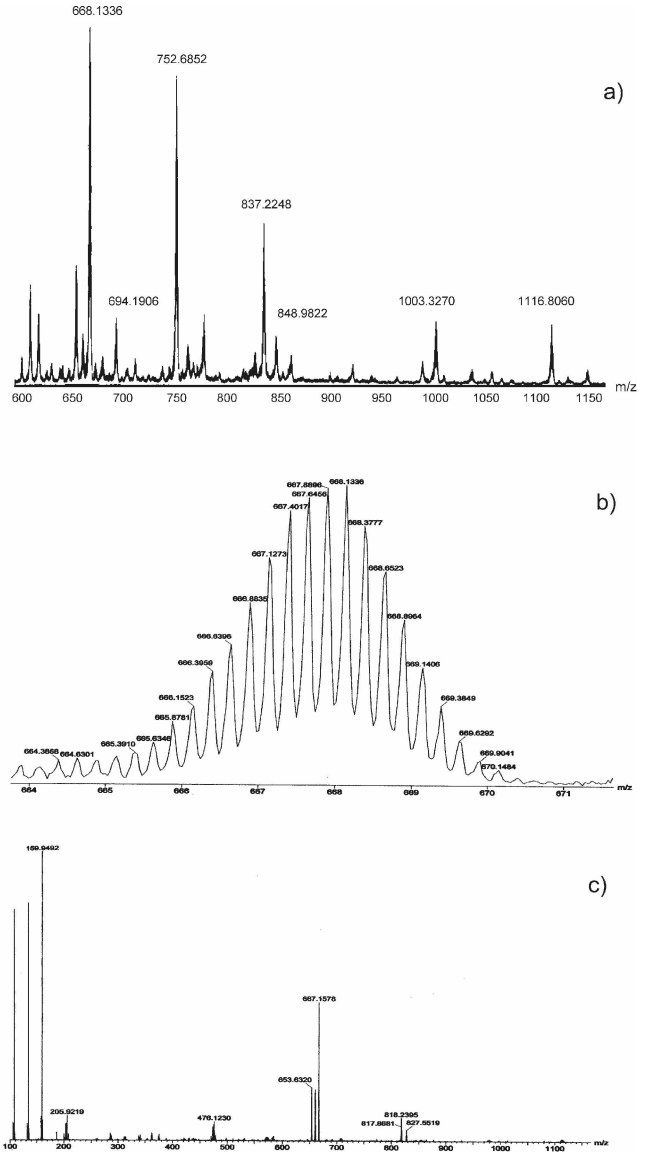

Figure 1. (a) Typical ESI-MS for $[PPh_4]_6\,\mathbf{2}$ salt, (b) characteristic isotope cluster observed for the $[\mathbf{2} + 2H]^{4-}$ anion, and (c) ESI-MS/MS for CID of a selected isotopologue ion for the $[\mathbf{2} + 2H]^{4-}$ anion.

(18) (a) Nikolaou, S.; Tomazela, D. M.; Eberlin, M. N.; Toma, H. E. *Transition Met. Chem.* **2008**, *33*, 1059–1065. (b) Moreira, E. Z.; de Moraes, L. A. B.; Eberlin, M. N.; Iamamoto, Y.; Nikolaou, S. *Polyhedron* **2008**, *27*, 2721–2729. (c) Tomazela, D. M.; Gozzo, F. C.; Mayer, I.; Engelmann, R. M.; Araki, K.; Toma, H. E.; Eberlin, M. N. *J. Mass Spectrom.* **2004**, *39*, 1161–1167. (d) Raminelli, C.; Prechtl, M. H. G.; Santos, L. S.; Eberlin, M. N.; Comasseto, J. V. *Organometallics* **2004**, *23*, 3990–3996. (e) Pereira, R. M. S.; Paula, V. I.; Buffon, R.; Tomazela, D. M.; Eberlin, M. N. *Inorg. Chim. Acta* **2004**, *357*, 2100–2106.

varies slightly upon selection for ESI-MS/MS experiments) was found to dissociate via collisions with argon (Figure 1c) mainly via the sequential losses of two neutral HNC molecules (probably from both CN end groups) to form the quadruply charged fragment anions of m/z 660.3978 and 653.6320 intercalated with the loss of a $[Fe(CN)_4]^-$ anion of m/z 159.9492 to form the triply charged fragment anions of m/z 818.2395 and 827.5519 (Figure 1c). The singly charged $[Fe(CN)_4]^-$ anions of m/z 159.9492 also fragment by the loss of CN radicals to form the fragment anions $[Fe(CN)_3]^-$ of m/z 132.9723 and $[Fe(CN)_2]^-$ of m/z 107.9678 (Scheme 2).

For $\mathbf{4}^{6-}$ and $\mathbf{6}^{6-}$, the intact multiprotonated or cationized species just described are also detected, for instance $[\mathbf{6} + 3H]^{3-}$ of m/z 839.1387 in Figure 2a, but both of them behaved uniquely since they display in their ESI-MS a prominent fragment ion (F1 in Scheme 2) arising, most probably, from the double protonated species via the cleavage of the cyanide wire (m/z 482.0373 in Figure 2a). These fragment ions also display typical clusters of isotopologue ions (Figure 2b) and dissociation chemistry (Figure 2c) similar to that observed for the intact protonated species (Scheme 2). Note that, similarly to the chemistry seen in Figure 1c (Scheme 2), the doubly charged isotopologue ion of m/z 481.5453 for the fragment F1 loses sequentially two molecules of HNC to form the fragments of m/z 468.0216 and 454.5146 intercalated with $[Fe(CN)_4]^-$ loss to form mainly the fragments of m/z 159.9492 and 749.1273.

Table 1. m/z Values of the Most Abundant Isotopologue Ion Observed via ESI-MS for the Anionic Complexes in Partially Protonated Species

		m/z	
salt	anionic complex	experimental	calculated
1	$[\mathbf{1} + 2H]^{4-}$	555.5257	555.5244
2	$[\mathbf{2} + 2H]^{4-}$	667.8896	667.8984
3	$[\mathbf{3} + 2H]^{4-}$	615.7596	615.7969
4	$[\mathbf{4} + 3H]^{3-}$	759.0780	759.0759
5	$[\mathbf{5} + 3H]^{3-}$	908.2923	908.2422
6	$[\mathbf{6} + 3H]^{3-}$	839.1387	839.1387
7	$[\mathbf{7} + 2H]^{3-}$	640.8422	640.8469

STM Measurements. STM determinations have sufficient spatial resolution to reveal the linear nature of the clusters. The images of the immobilized heptanuclear complex $\mathbf{3}^{6-}$ show elongated features that clearly contrast with the globular images acquired for the reference trinuclear compound, *trans*-$[(MeOpy)_4Ru^{II}\{(\mu\text{-}CN)Fe^{III}(CN)_5\}_2]^{4-}$ (Figure 3). The Auger electron spectroscopy spectra of these surfaces clearly indicate the presence of the molecules as can be assessed from the characteristic peaks corresponding to Ru and Fe elements (see Supporting Information, Figure S1). The absence of P peaks shows that no Ph_4P^+ counterions are adsorbed. Comparison of these spectra with the ones for the free-molecule surface allows noticing the enhancement of the C and N peaks in detriment of the S peak, confirming the presence of the complex in the surface.

The statistical distribution of species over the surface has a sharp maximum at a length of 3.5 nm (see Supporting Information, Figure S2), in good agreement with the

Scheme 2. (Top) General Dissociation Pathway Observed via ESI-MS/MS for the Species $[\mathbf{1}-\mathbf{6} + 2H]^{4-}$; (Bottom) General Dissociation Pathway for the Species $[\mathbf{4}-\mathbf{5} + 2H]^{4-}$ Leading to the Doubly Charged Fragment Ions F1

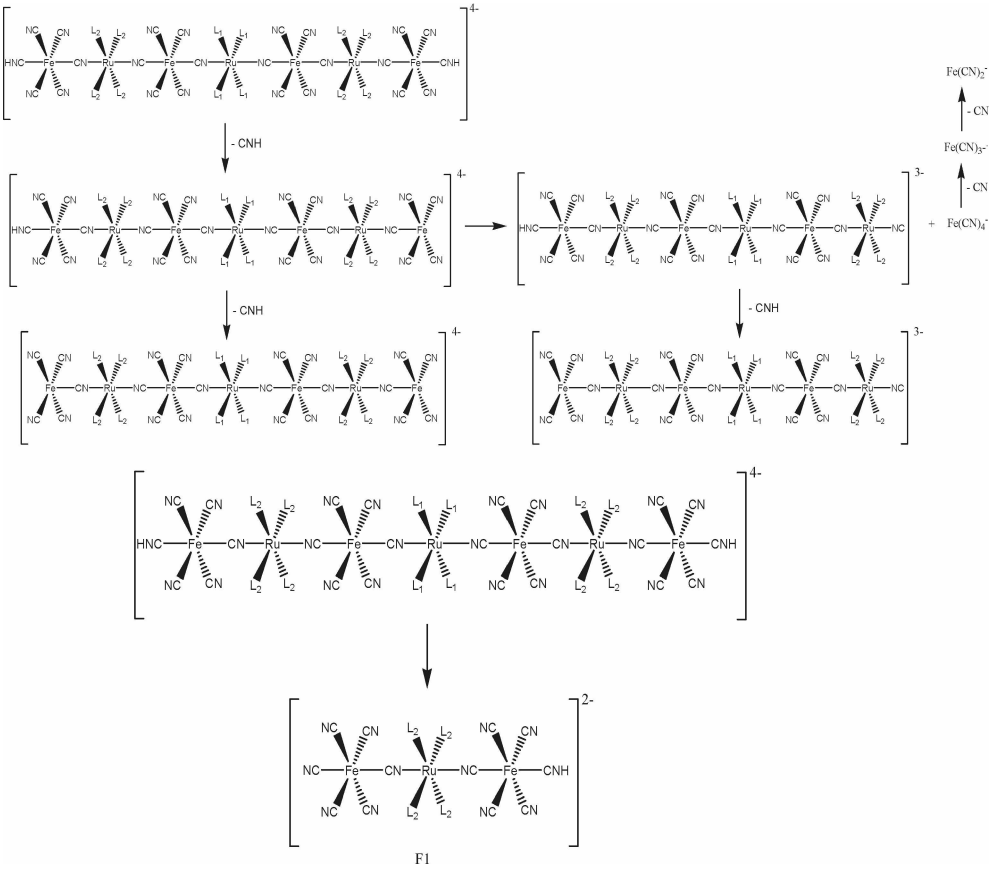

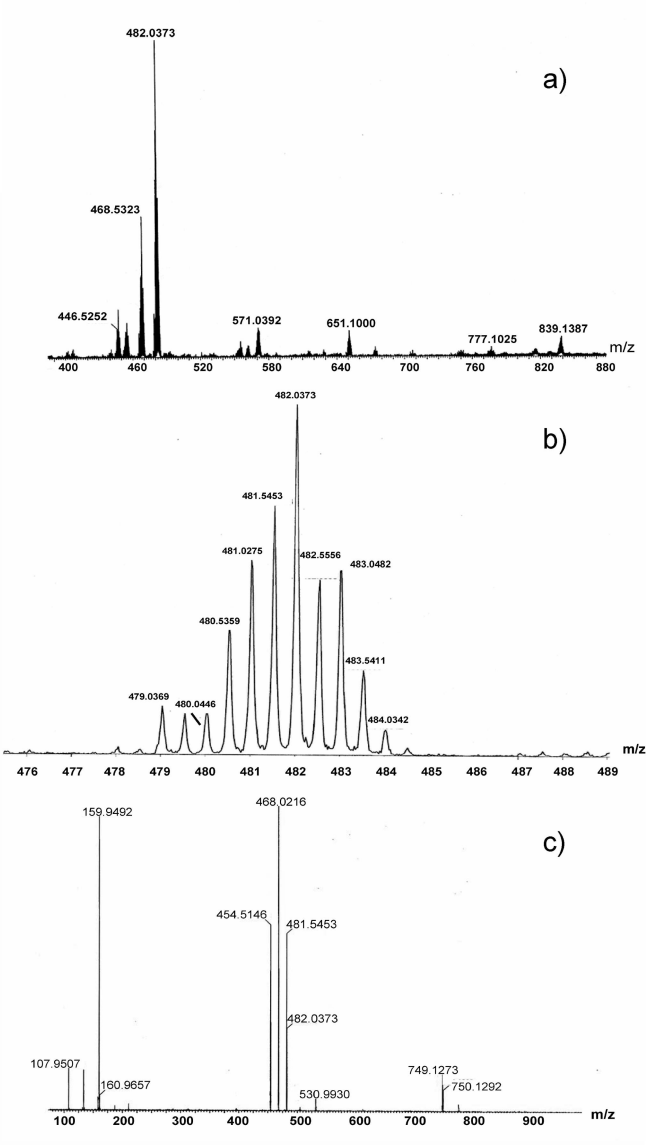

Figure 2. (a) Typical ESI-MS for $[PPh_4]_6$**6** salt, (b) characteristic isotope cluster observed for the F1 fragment ion from $\mathbf{6}^{6-}$ (see Scheme 2), and (c) ESI-MS/MS for CID of a selected isotopologue ion for the F1 ion of *m*/*z* 481.5453.

expected length (approximated from the observed distances in the trinuclear complexes X-ray structures[5]) of about 3.6 nm for this molecule. This distribution also shows a tail to larger lengths with a local maximum at 7.5 nm, evidencing heptamer association at the surface, probably mediated by H-bonds between the terminal cyanides. A closer inspection at the dimensions of these features shows a width that ranges between 1.7 and 2 nm in concordance with the expected value of about 1.6 nm. Cyclic voltammetry measurements of the surfaces with the complexes adsorbed, also show waves corresponding to the Ru(II)/Ru(III) and Fe(III)/Fe(II) redox couples, indicating that these compounds remain electroactive after immobilization (see Supporting Information, Figure S3).

Electrochemistry. Cyclic voltammograms and square wave voltammograms of these complexes exhibit several reversible redox processes corresponding to the Fe(III)/Fe(II) and Ru(II)/Ru(III) redox couples. Figure 4 shows measurements for some of the reported complexes (for the remaining ones see Supporting Information, Figure S4) while the experimental observed $E°$ values are listed in Table 2.

For the pentanuclear complex **7**, five resolved redox processes are distinguished in water (see Supporting

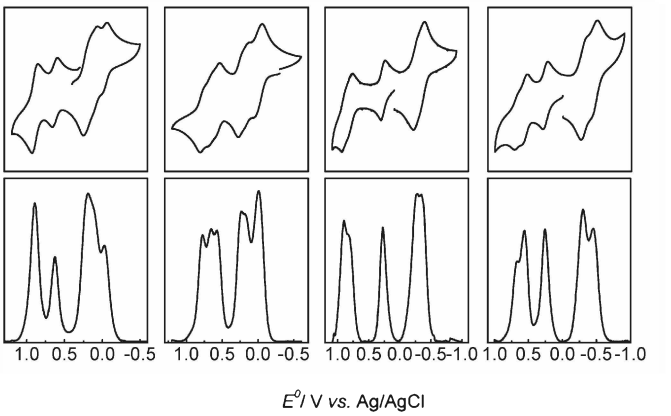

Figure 4. Cyclic voltammetry (top) and square wave voltammetry (bottom) for complexes **1** and **3** in water and **4** and **6** in methanol, from left to right respectively.

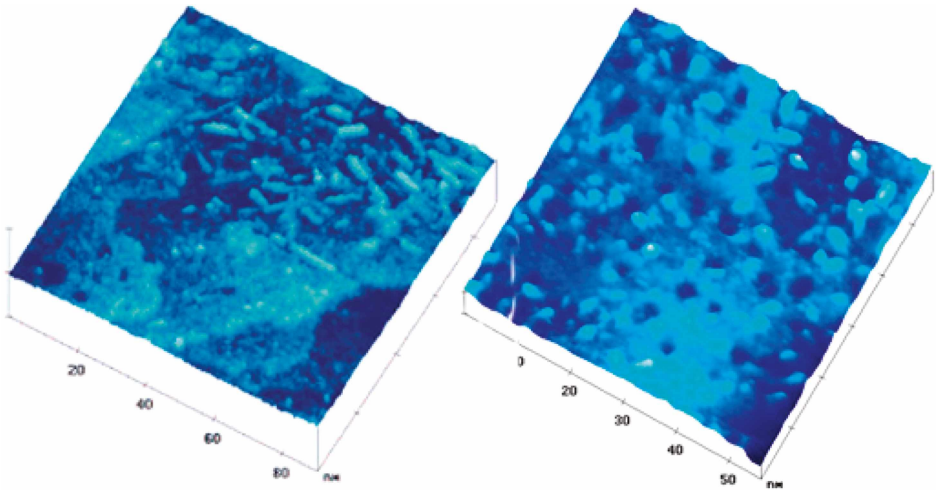

Figure 3. STM images for the immobilized heptanuclear compound **3** (left) and related trinuclear compound (right) over cysteamine derivatized Au surfaces.

Table 2. Electrochemistry Data for Complexes **1**–**7**

complexes (RuL_4 pattern)	solvent	E°/V (ΔE_p/mV) outer $Ru^{II/III}$ couples	inner $Ru^{II/III}$ couple	$Fe^{III/II}$ couples
1 (py-MeOpy-py)	water	0.89 (80)	0.63 (70)	0.21 (~100), 0.09 (~60), −0.03 (~60)
2 (*t*Bupy-MeOpy-*t*Bupy)	water	0.80 (100)	0.64 (70)	0.17 (~80), 0.01 (~100)
3 (MeOpy−MeOpy−MeOpy)	water	0.57(~70) 0.65 (~70)	0.77 (~60)	0.23 (~60), 0.17 (~60), −0.01 (~100)
4 (py-DMAP-py)	methanol	0.83 (~60) 0.91 (~60)	0.28 (60)	−0.26 (~60), −0.34 (~60)
5 (*t*Bupy-DMAP-*t*Bupy)	methanol	0.75 (~60) 0.84 (~80)	0.21 (70)	−0.17 (70), −0.35 (100)
6 (MeOpy-DMAP-MeOpy)	methanol	0.56 (~70) 0.67 (~60)	0.26 (70)	−0.30 (80), −0.45 (80)
7 (tBupy-*t*Bupy)	water	0.68 (70) 0.87 (90)		0.19 (~70), 0.14 (~70), 0.00 (~60)

Information, Figure S4), attributed to the whole set of expected metal-centered redox processes. The processes at 0.87 and 0.68 V correspond to the oxidation of the Ru(II) centers, while the other three processes correspond to the reduction of the Fe(III) moieties.

The electrochemistry of the heptanuclear complexes is more complex because of the increased number of redox active centers. The Ru(II)/Ru(III) couples are observed at potential values close to the observed in the corresponding trimer (0.85, 0.75, 0.60, and 0.25 V for py, tBupy, MeOpy and DMAP, respectively). The redox processes at lower potentials correspond to the consecutive overlapped reductions of the Fe centers. The electrochemistry of **1**−**3** and **7** were measured in water, as in this solvent the reduction potential of the hexacyanoferrate moieties are higher and a larger interaction between the centers is expected.[5] For **4**−**6**, methanol was chosen instead, to avoid possible redox isomerization between the Ru^{II}-$(DMAP)_4$ and the Fe(III) center, as the latter redox potential shift cathodically in water.

Electronic Spectroscopy. The electronic spectra of **1**−**7** share several features with the trinuclear precursors.[5] They exhibit an intense band in the UV region arising from the $d_\pi(Ru^{II}) \rightarrow \pi^*_L$ metal-to-ligand charge-transfer (MLCT) transitions within the cromophores $\{Ru^{II}L_4\}$ and a set of bands in the NIR region originating from $d_\pi(Ru^{II}) \rightarrow d_\pi(Fe^{III})$ MM′CT transitions (Figure 5 and Supporting Information, Figure S6). Table 3 summarizes the relevant characteristics of these spectra.

The spectrum of **7** displays an intense $d_\pi(Ru^{II}) \rightarrow \pi^*_L$ MLCT band at 27.8 × 10^3 cm^{-1}, roughly at the same energy observed in the related trinuclear compound *trans*-$[(t\text{Bupy})_4Ru^{II}\{(\mu\text{-CN})Fe^{III}(CN)_5\}_2]^{4-}$. Its extinction coefficient of 45.4 × 10^3 M^{-1} cm^{-1}, nearly doubles the observed in the above-mentioned trinuclear species. The NIR spectrum is dominated by an MM′CT band at 8.1 × 10^3 cm^{-1} with an incipient shoulder at the high energy side. This transition is red-shifted if compared to the trinuclear complex bearing the same kind of pyridine.

The spectra of the heptanuclear complexes **1**−**6**, also show MLCT bands in the UV−vis region. Their extinction coefficients roughly scale up with the number of $\{Ru^{II}L_4\}$ cromophores whereas their energies resemble those of the analogous transitions in the corresponding trinuclear precursors. The most interesting feature is the presence of the MM′CT bands between 5.0 × 10^3 and 10.0 × 10^3 cm^{-1}. Two bands appear clearly resolved for

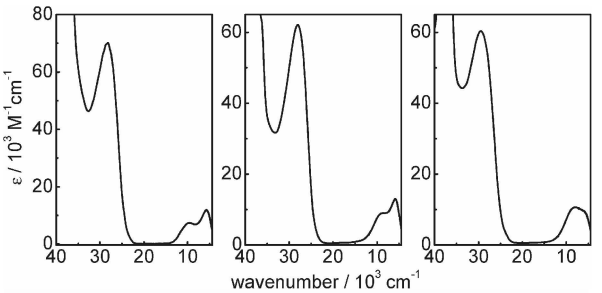

Figure 5. From left to right, electronic spectra for **4**−**6** in methanol.

Table 3. Spectroscopic Data for Complexes **1**−**7** in Methanol

Complexes	MLCT $d_\pi Ru(II) \rightarrow \pi^*_L$ wavenumber/ 10^3 cm^{-1} (ε /M^{-1} cm^{-1})	MM′CT $d_\pi Ru(II) \rightarrow d_\pi Fe(III)$ wavenumber/ 10^3 cm^{-1} (ε /M^{-1} cm^{-1})
1	28.1 (59100)	7.8 (15700) 10.1 (11700) [a]
2	27.9 (68100)	7.7 (17200) 9.7 (12500) [a]
3	29.2 (59800)	7.3 (18900) 9.1 (14000) [a]
4	28.2 (71100)	5.7 (13000) 9.6 (8500)
5	28.1 (62100)	5.9 (13000) 9.0 (9000)
6	29.4 (60300)	6.0 (9600) [a] 8.1 (10700)
7	27.8 (45400)	8.1 (9300) 9.7 (7400) [a]

[a] Observed as a shoulder.

4−**6** with $\{Ru^{II}(DMAP)_4\}$ as the central moiety as expected for a system with two Ru(II) donors of very different energies.

The low redox potential of the Ru(II) centers in the $\{Ru^{II}(DMAP)_4\}$ core allowed for a complementary spectroscopic characterization in methanol of the one-electron oxidized species derived from **4**−**6**. They show the characteristic $\pi(DMAP) \rightarrow d_\pi(Ru^{III})$ LMCT bands at about 15.0 × 10^3 cm^{-1}, expected for the $\{Ru^{III}(DMAP)_4\}$ cromophore.[15] Upon oxidation, the low energy MM′CT bands disappear whereas the high energy ones are still observable (see Supporting Information, Figure S7).

Discussion

In a previous report[5] we showed that hexacyanoferrate(III) can be employed to substitute the halides in *trans*-$Ru^{II}L_4X_2$

species with accurate control of product nuclearity. This process yielded trinuclear species with terminal cyanide groups that we use now as the nucleophiles in a second round of substitution reactions on the same type of molecules. The use of a large excess of trinuclear anion with respect to the ruthenium mononuclear building block affords heptanuclear complexes as the main products, though size exclusion chromatography purification is still needed to ensure purity. Through the same procedure we isolated the pentanuclear complex **7**. In the preparation of the trinuclear complexes, the product also behaves as a nucleophile toward *trans*-$Ru^{II}L_4X_2$ to afford a tetranuclear complex $\{Fe^{III}-Ru^{II}-Fe^{III}-Ru^{II}\}$, which is end-capped to yield a pentanuclear complex such as **7**.

Regrettably, we were not able to grow single crystals of any of these oligomers, probably because of the large number of solvent molecules associated to them through the strong interactions with the terminal cyanides. However, the mass spectrometric data conclusively confirms their nuclearity. There are only a few examples in the literature where discrete high dimension clusters could be characterized with mass spectrometry techniques.[19] Normally, the lability of the gaseous ion precludes its detection in intact forms. Using a soft ionization technique, ESI, we have been able to observe our polynuclear multiply charged anions as intact species and therefore intrinsically stable gaseous species with a low degree of dissociation in spite of their high charge density (alleviated partially during ESI via protonation and/or cationization) and the presence of several relatively labile terminal cyanides. For most complexes, the major anions detected correspond to the salt anion with partial charge reduction because of protonation as shown by their m/z values, their characteristic isotopic patterns, mostly due to various Ru and/or Fe elements in their composition, and their characteristic dissociation patterns. ESI-MS/MS provided further structural characterization via characteristic and structurally diagnostic dissociation channels.

The excellent resolution obtained in the STM images of the surface attached clusters leaves no doubt about their linear nature, even more when compared to the globular shape of the trinuclear species attached to the surface. The constrained robust geometry of the precursors and the bulkiness of the L ligands coordinated to the Ru(II) centers drive the reaction exclusively to the linear arrangement, and the STM images constitute a unique evidence of the architecture of these clusters.[20]

Scheme 3. Qualitative Description of the Expected MM′CT in the heptanuclear complexes NIR spectra

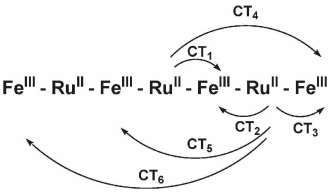

Scheme 4. Simplified Picture of the Heptanuclear Complexes from a Spectroscopic Point of View, Showing Their Decomposition in a Superposed Sets of Trinuclear Units

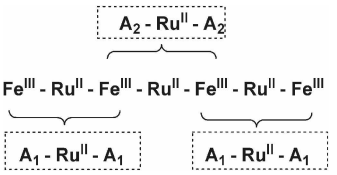

For a molecular wire, the property of interest is the electronic coupling between the terminal units. In this sense, the electrochemical behavior of the clusters appears as a valuable probe. The splitting of redox waves arising from chemically equivalent sites constitutes an evidence of long-range communication once other contributions are taken into consideration.[21] We[5] and others[3,4,8,22] have successfully used this tool to explore the degree of electronic communication in trinuclear cyanide bridged compounds and in higher oligomers,[14] and we also employ it here to evaluate the presence of long-range interaction in these clusters. To avoid solvent effects,[23] we will limit our comparisons to systems measured in the same solvent.

In the cyclic voltammetry measurements of the pentanuclear complex **7** in water, the two anodic waves, separated by 190 mV, correspond to both Ru(II)/Ru(III) redox couples. This non-negligible $E°$ splitting ($\Delta E°$) evidence electronic communication between the $\{Ru(t\text{Bupy})_4\}$ moieties through the hole-type $\{\text{-}NCFe^{III}(CN)_4CN\text{-}\}$ bridge. The three cathodic processes observed in this species can be reliably attributed to the three Fe(III)/Fe(II) couples. The first two waves, slightly split (ca. 50 mV), arise from the terminal Fe moieties as can be inferred from the similar $E°$ value (0.19 and 0.14 V) with respect to the first Fe(III)/Fe(II) reduction at 0.23 V observed in the trinuclear compound *trans*-$[(t\text{Bupy})_4L_4Ru^{II}\{(\mu\text{-}CN)Fe^{III}(CN)_5\}_2]^{4-}$,[5] suggesting an analogous environment for these Fe centers in both compounds. The remaining redox wave at 0 V corresponds to the reduction of the central Fe fragment.

For the heptanuclear complexes **1**−**6**, the first oxidation process in **1** and **2** around 0.6 V can be readily assigned to the Ru(II)/Ru(III) couple of the central $\{Ru(MeOpy)_4\}$ core because of the lower $E°$ value expected for this fragment. The following anodic process corresponds to the simultaneous oxidation of the two equivalent $\{RuL_4\}$ outer fragments, indicating little interaction between these centers. For **4**−**6**

(19) (a) Schalley, C. A.; Muller, T.; Linnartz, P.; Witt, M.; Schafer, M.; Lutzen, A. *Chem.—Eur. J.* **2002**, *8*, 3538–3551. (b) Alves, W. A.; Cerchiaro, G.; Paduan, A.; Tomazela, D. M.; Eberlin, M. N.; Ferreira, A. M. D. *Inorg. Chim. Acta* **2005**, *358*, 3581–3591. (c) Toma, S. H.; Nikolaou, S.; Tomazela, D. M. Eberlin, M. N.; Toma, H. E. *Inorg. Chim. Acta* **2004**, *357*, 2253–2260. (d) Hasenknopf, B.; Lehn, J. M.; Boumediene, N.; DupontGervais, A.; VanDorsselaer, A.; Kneisel, B.; Fenske, D. *J. Am. Chem. Soc.* **1997**, *119*, 10956–10962. (e) Toma, H. E.; Nikolaou, S.; Eberlin, M. N.; Tomazela, D. M. *Polyhedron* **2005**, *24*, 731–738.

(20) The orientation of the cyanide bridge is expected from the connectivity in the precursors. In previous work we did not find isomerization of the cyanide bridge and in one case we have prepared the two possible isomers (see ref 5). The properties of the two isomers are quite distinctive, especially their redox behavior. Isomerization of the bridge results in an increase in the redox potential of the $Ru^{II/III}$ couple, while the $Fe^{III/II}$ couples become more irreversible because of the lability of the Fe−N(nitrile) bond. Our exploration of the redox properties of the complexes reported here show no evidence of bridge isomerization.

(21) (a) Flanagan, J. B.; Margel, S.; Bard, A. J.; Anson, F. C. *J. Am. Chem. Soc.* **1978**, *100*, 4248–4253. (b) Richardson, D. E.; Taube, H. *J. Am. Chem. Soc.* **1983**, *105*, 40–51. (c) Sutton, J. E.; Taube, H. *Inorg. Chem.* **1981**, *20*, 4021–4023.

(22) (a) Coe, B. J.; Meyer, T. J.; White, P. S. *Inorg. Chem.* **1995**, *34*, 3600–3609. (b) Sheng, T. L.; Vahrenkamp, H. *Eur. J. Inorg. Chem.* **2004**, 1198–1203.

(23) D'Alessandro, D. M.; Keene, F. R. *Dalton Trans.* **2004**, 3950–3954.

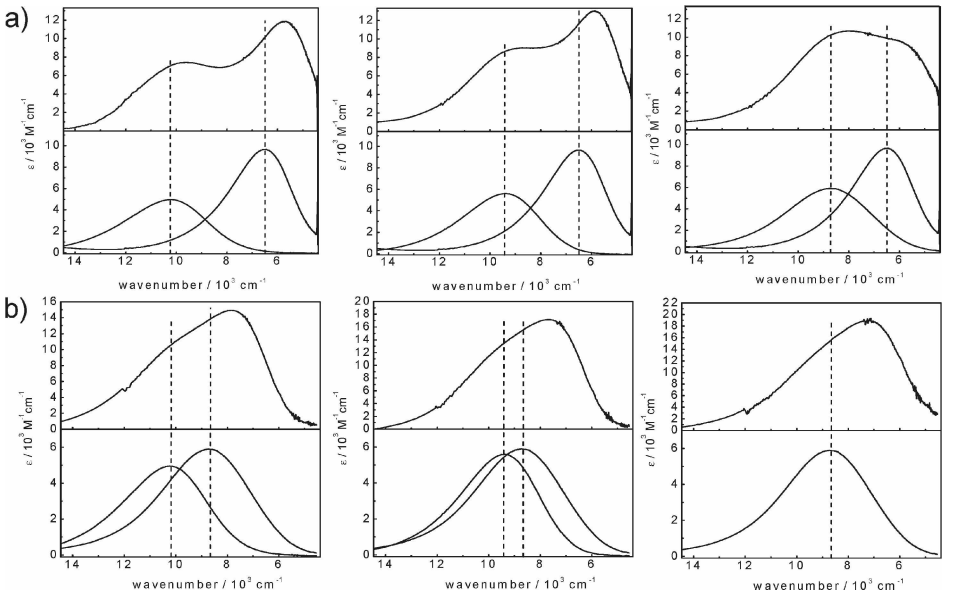

Figure 6. (a) Top: NIR electronic spectra in methanol of complexes **4**–**6** (left to right). Bottom: Superposed NIR electronic spectra in methanol of the trinuclear complexes built in the corresponding heptanuclear complexes. (b) Top: NIR electronic spectra in methanol for complexes **1**–**3** (left to right). Bottom: Superposed NIR electronic spectra in methanol of the trinuclear complexes built in the corresponding heptanuclear complexes.

containing {Ru(DMAP)$_4$} as the central core, the oxidation of the outer {RuL$_4$} fragments are well resolved. The observed $\Delta E°$ values for these couples are 80, 90, and 110 mV for **4**, **5**, and **6**, respectively, showing a gradual enhancement of the long-range interaction. Finally, in **3** with identical {Ru(MeOpy)$_4$} fragments, three waves at 0.57, 0.65, and 0.77 V are observed. The first two processes appear at a potential close to the observed for the Ru(II)/Ru(III) couple in *trans*-[(MeOpy)$_4$Ru^{II}{(μ-CN)Fe^{III}(CN)$_5$}$_2$]$^{4-}$;[5] hence we assign them as the outer {Ru(MeOpy)$_4$} fragments oxidation. The remaining anodic wave arises from the central {Ru(MeOpy)$_4$}, Ru(II)/Ru(III) couple. For this complex, two reduction waves at 0.23 and 0.17 V are observed, and we assign them as the outer Fe fragments reduction.

The previous results show significant splitting of the redox potential for {RuL$_4$} centers more than 2.0 nm apart[24] in complexes **3**, **4**, **5**, and **6**, but not for complexes **1** and **2**. Splitting of the redox potential for the iron moieties at the same distance is also observed in **7**. Redox potential splitting for centers at similar distances has been observed in ruthenium complexes linked by bis-ethynyl aryl groups[25,26] and a phenylcyanamido-bridge[26] and in multinuclear Ru(II)-polypyridine rack-type complexes,[14] all systems with small attenuation of the electronic interaction with the distance.[14,26,27] The magnitude of the splitting depends on the properties of oligomer constituents. As the redox potential of the outer {RuL$_4$} moiety gets closer to the one of the central fragment, the $\Delta E°$ values increase (80, 90, and 110 mV for **4**, **5**, and **6**). This effect is also noticeable in **3** where the three {RuL$_4$} fragments are identical. In fact, this is the only member of the family where the two reduction processes at the terminal Fe fragments around 0.2 V appear slightly resolved with a splitting of 60 mV. This may suggest an electronic communication at distance of more than 3.0 nm. This is the only complex where this remote Fe–Fe redox potential split is observed and may indicate that a three identical {RuL$_4$} fragments pattern results in a better electronic communication along the molecule. It appears striking that the inner Fe reduction processes, closer in distance, are not resolved. It could be possible that the reduction of the terminal Fe fragments may induce the decoupling of the inner Fe fragments. However, it is true that this effect is more the exception than the rule and illustrates that a better understanding of the electronic interaction in these systems is required for the rational design of these linear molecules with long distance interactions.

The NIR spectra of these oligomers evidence several Ru(II) → Fe(III) MM′CT bands. A quantitative interpretation of these bands using a generalized Mulliken–Hush[28] multiple state treatment (successfully employed for the related trinuclear species[6]) is ruled out because of the large number of states that should be included for the large molecules discussed in this work, but a qualitative analysis of these electronic transitions is still valuable to evaluate the metal–metal interaction degree.

In the most simplified description, six $d_\pi(Ru^{II}) \rightarrow d_\pi(Fe^{III})$ MM′CT single excitation transitions are expected for the heptanuclear complexes (Scheme 3), but the presence of {RuL$_4$} fragments with very different properties makes the assignment of these transitions easier. For **4**–**6**, two MM′CT bands are well resolved.

The lower energy band can be safely assigned as the MM′CT transitions that involve the central {Ru^{II}(DMAP)$_4$}, which behaves as a better donor. The energy of this transition is almost the same for these three compounds, about 6.0×10^3 cm^{-1}. The remaining band appears at 9.6×10^3, 9.0×10^3, and 8.1×10^3 cm^{-1} for **4**, **5**, and **6**, respectively. This energy trend correlates well with the expected donor strength of the outer {Ru^{II}L$_4$} moieties.

(24) We estimate the distance between the redox centers as multiples of the Fe–Ru distance of 5.05 Å observed in the trinuclear compounds.

(25) (a) Fraysse, S.; Coudret, C.; Launay, J. P. *J. Am. Chem. Soc.* **2003**, *125*, 5880–5888. (b) Hoshino, Y.; Suzuki, T.; Umeda, H. *Inorg. Chim. Acta* **1996**, *245*, 87–90.

(26) Fabre, M.; Bonvoisin, J. *J. Am. Chem. Soc.* **2007**, *129*, 1434–1444.

(27) Launay, J. P. *Chem. Soc. Rev.* **2001**, *30*, 386–397.

(28) Cave, R. J.; Newton, M. D. *Chem. Phys. Lett.* **1996**, *249*, 15–19.

The NIR spectra of the one electron oxidized **4**−**6** strongly support the previous assignments, as the low energy MM′CT band (involving $\{Ru^{II}(DMAP)_4\}$ as the donor fragment), disappears upon oxidation (see Supporting Information, Figure S7). The remaining features still correspond to the overlapping MM′CT transitions arising from the reduced outer $\{Ru^{II}L_4\}$ fragments. A simple model to interpret the absorption spectra of these oxidized complexes assumes that it corresponds to the superposition of those of two *trans*-$[L_4Ru^{II}\{(\mu\text{-}NC)Fe^{III}(CN)_5\}_2]^{4-}$ species coordinated to a $\{Ru^{III}DMAP_4\}$ fragment. The energy of the MM′CT band is shifted to the red when compared to the same transition in the corresponding trinuclear compound,[5] as expected for the coordination to the electron withdrawing $\{Ru^{III}(DMAP)_4\}$ moiety. Interestingly, upon oxidation of the central Ru(II) to Ru(III), no evidence of a $d_\pi(Ru^{II}) \rightarrow d_\pi(Ru^{III})$ MM′CT transition is observed. Either the intensity of this band is too low to be observed or the molecular orbital involved in the one-electron oxidation in the $\{Ru(DMAP)_4\}$ center is mainly localized at the d_{xy} Ru orbital orthogonal to the extended d_π (d_{xz}, d_{yz}) backbone that mixes the metallic centers. If interaction between the d_{xz}, d_{yz}, and the cyanide orbitals is strong enough, then the latter is expected.

The MM′CT bands in **1**−**3** exhibit a similar pattern, except that the two components appear less resolved as the $E°$(Ru(III)/Ru(II)) associated with the central $\{Ru^{II}(MeOpy)_4\}$ moiety is scarcely different from the $E°$(Ru(III)/Ru(II)) of the outer $\{Ru^{II}L_4\}$ moieties. For qualitative purposes, we can describe the heptanuclear compounds (at least from the spectroscopic point of view) as a superposition of trinuclear compounds (Scheme 4).

This is a reasonable zero-order approximation provided that the degree of mixing in these systems is low. For **4**−**6** (central $\{Ru(DMAP)_4\}$ core), the MM′CT band profile is approximately reproduced by the superposition of the experimental MM′CT bands of the two trinuclear components, although shifted to lower energies (Figure 6a). The approximation seems to break down for **1**−**3**, (central $\{Ru(MeOpy)_4\}$ moiety) where the MM′CT band profiles cannot be satisfactorily reproduced by the mere superposition of trinuclear MM′CT bands, suggesting an increased degree of interaction between the trinuclear fragments (Figure 6b). A similar behavior can also be observed for the pentanuclear complex $\mathbf{7}^{5-}$ (Supporting Information, Figure S8), which shows two extensively overlapped bands ascribed to the two possible MM′CT transitions involving the two different Fe(III) acceptor sites present in its structure.

The different spectroscopic behavior observed for the two groups of heptamers, **1**−**3** and **4**−**6**, suggests a larger interaction between the metal centers in the former group, probably because of an improved energy match of the three d_π (Ru^{II}) orbitals. This hypothesis is in agreement with the electrochemistry behavior of **3**, which shows split couples for the outer Fe(III) fragments reduction.

Conclusions

The facile preparation, solubility, and stability in solution of a family of cyanide bridge trinuclear complexes allowed us to use them as starting materials for the synthesis of increased nuclearity complexes. The resulting linear oligomers are also stable in solution and could be characterized in different redox states. The spectroscopic and electrochemical properties of the oligomers reported here show evidence of significant electronic communication between metal centers along the chain granting further exploration. The flexibility of the synthetic approach should allow us to prepare systems of different nuclearities with precise control of their composition where more insights on the extent of the communication could be attained.

Acknowledgment. The authors thank the University of Buenos Aires, the Consejo Nacional de Investigaciones Cientificas y Técnicas (CONICET), and the brazilian science foundations CNPq and FAPESP for funding. We are also grateful to Johnson Matthey for a generous loan of $RuCl_3$. P.A., L.B.V., L.D.S., and R.C.S. are members of the scientific staff of CONICET.

Supporting Information Available: Further details are given in Figures S1−S8. This material is available free of charge via the Internet at http://pubs.acs.org.